An artificial aquatic polyp that wirelessly attracts, grasps, and releases objects

Marina Pilz da Cunha[a,b], Harkamaljot S. Kandail[c], Jaap M. J. den Toonder[b,d,1], and Albert P. H. J. Schenning[a,b,1]

[a]Laboratory of Stimuli-responsive Functional Materials & Devices, Department of Chemical Engineering and Chemistry, Eindhoven University of Technology, 5600 MB Eindhoven, The Netherlands; [b]Institute for Complex Molecular Systems, Eindhoven University of Technology, 5600 MB Eindhoven, The Netherlands; [c]WMG, University of Warwick, Coventry CV4 7AL, United Kingdom; and [d]Department of Mechanical Engineering, Eindhoven University of Technology, 5600 MB Eindhoven, The Netherlands

Edited by David A. Weitz, Harvard University, Cambridge, MA, and approved June 17, 2020 (received for review March 12, 2020)

The development of light-responsive materials has captured scientific attention and advanced the development of wirelessly driven terrestrial soft robots. Marine organisms trigger inspiration to expand the paradigm of untethered soft robotics into aqueous environments. However, this expansion toward aquatic soft robots is hampered by the slow response of most light-driven polymers to low light intensities and by the lack of controlled multishape deformations. Herein, we present a surface-anchored artificial aquatic coral polyp composed of a magnetically driven stem and a light-driven gripper. Through magnetically driven motion, the polyp induces stirring and attracts suspended targets. The light-responsive gripper is sensitive to low light intensities and has programmable states and rapid and highly controlled actuation, allowing the polyp to capture or release targets on demand. The artificial polyp demonstrates that assemblies of stimuli-responsive materials in water utilizing coordinated motion can perform tasks not possible for single-component devices.

soft robotics | light-responsive polymers | magnetic responsive polymers

Inspired by nature's intricate organisms, the field of soft robotics has advanced toward fully untethered devices triggered into action by external stimuli such as light, pH, and magnetic fields (1, 2). Recent developments mimic terrestrial organisms and demonstrate remotely controlled locomotion and object manipulation (3). However, centimeter-sized, wirelessly driven, stimuli-responsive soft robots that operate underwater are rarely reported (4–6), and fast actuation of stimuli-responsive polymers in water, without requiring high-intensity lasers, remains complicated. Expansion toward underwater untethered soft robotics challenges the current status of stimuli-responsive materials, calling for soft actuators with fast responses to low-intensity light, stability of multiple deformation states, and adaptability to diverse environments (7). An additional ambition is the elimination of the external tethering usually required to guide aquatic soft robotic grippers to targets (8–11). Taking inspiration from the motion freedom and adaptability of aquatic species may provide promising approaches to the development of wirelessly controlled, stimuli-responsive soft robots that interact with the environment and perform functional tasks such as grasping and release of targets.

Smart soft polymeric materials with responses to light and magnetic fields present a wireless approach to control the actuation of devices in enclosed spaces (12). Light is a particularly promising stimulus, being remotely controlled and providing high spatiotemporal resolution (13). Currently, the dominant stimuli-responsive materials employed in underwater applications are hydrogels, acting on changes in ambient temperature, light, or pH to trigger swelling/deswelling-driven actuation (14–16). As hydrogel materials rely on absorption and release of water, their actuation is often sensitive to contaminants such as charged species which can affect swelling/deswelling-driven actuation. Light-driven motion of centimeter-sized hydrogel actuators in water is often slow, being dictated by gradual diffusion processes, lacking facile motion reversibility (17), or requiring a constant stimulus (pulsed light) to retain an actuated state (18). Liquid crystal polymers (LCPs) doped with photoswitches, commonly azobenzene derivatives, are often employed in fast-responding light-driven actuators acting in dry environments (19, 20); however, their exploration for underwater systems is still in its infancy (4, 21, 22). Light-responsive grippers based on LCPs have been previously demonstrated (23), but current examples are only active in dry environments and rely on constant illumination to retain their deformed open state, so the geometry of a nonilluminated state cannot be programmed. Recently, liquid crystal gels have been utilized as untethered actuators operating via light to perform locomotion and swimming in aquatic environments, requiring high-intensity lasers and high temperature for fast, large-amplitude actuation (24).

In marine environments, organisms often rely on ocean currents to bring targets (nutrients) to their vicinity, but other animals such as coral polyps (Fig. 1*A*) have been observed to induce currents themselves through coordinated motion to aid their survival (25–27). Inspired by the motion and design of such marine organisms, we present a surface-anchored aquatic gripper capable of attracting and grasping suspended objects. This artificial polyp is composed of two active sections, the grasping "arms," composed of two photoactive liquid crystalline polymer

Significance

Wirelessly controlled, multitasking soft devices active in aqueous environments are highly required for applications in microfluidics and organ-on-a-chip and as medical devices. Inspired by marine organisms, we present an approach to achieve such devices by utilizing stimuli-responsive material assemblies capable of untethered object manipulation in an enclosed aqueous environment. Our soft robot assembly integrates a magnetically controlled stem with a light-responsive gripper with unmatched speed, insensitivity to contaminants, and high control of actuation underwater at low light intensities. The independent device segments can be orthogonally controlled to realize different tasks such as attracting, capturing, and releasing targets in an aqueous environment, demonstrating the significance of actuator assemblies in the fabrication of multifunctional soft devices operating underwater.

Author contributions: M.P.d.C., H.S.K., J.M.J.d.T., and A.P.H.J.S. designed research; M.P.d.C. and H.S.K. performed research; M.P.d.C. and H.S.K. analyzed data; and M.P.d.C., H.S.K., J.M.J.d.T., and A.P.H.J.S. wrote the paper.

The authors declare no competing interest.

This article is a PNAS Direct Submission.

[1]To whom correspondence may be addressed. Email: j.m.j.d.toonder@tue.nl or A.P.H.J. Schenning@tue.nl.

This article contains supporting information online at https://www.pnas.org/lookup/suppl/doi:10.1073/pnas.2004748117/-/DCSupplemental.

First published July 13, 2020.

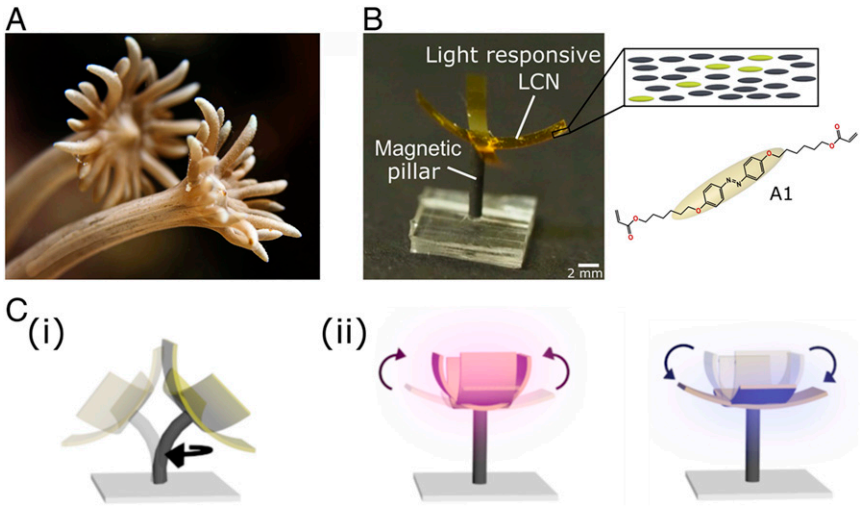

Fig. 1. Design of artificial aquatic polyp. (*A*) Photograph of a marine polyp, reproduced with permission from photographer Robin Jeffries. (*B*) The artificial polyp inspired by the design of marine polyps. The device is composed of two LCN films with planar alignment that operate as the device's grasping "arms." The LCNs are connected to a flexible PDMS/iron oxide pillar with a drop of UV-curable glue. The LCN is a highly cross-linked network containing azobenzene diacrylate mesogens, A1. (*C*, *i*) Upon rotation of a magnet underneath the polyp, the structure undergoes a bending and rotational motion which when submerged in a fluid causes an effective flow. (*C*, *ii*) Upon UV light irradiation the polyp is made to close and blue light reversibly opens the structure.

films, and a flexible stem of polydimethylsiloxane (PDMS) doped with magnetic iron oxide particles (Fig. 1*B*). Hence, we integrate two stimuli-responsive materials which serve different functionalities and can be wirelessly and independently controlled; namely, light activates the liquid crystal network (LCN) gripper and a magnetic field induces rotational motion of the flexible stem to create flow. Previously, magnetic particles have been incorporated into hydrogel-based microgrippers (28, 29) and thermoplastic polyurethane films (30) so that magnetic guidance can be used to direct and control the location of the device. However, magnetic setups required to accurately control such aquatic microgrippers are usually bulky, limiting the versatility of the soft robot (5, 31). Our artificial polyp can be actuated with a compact setup, only requiring a rotating magnet near its location. Detailed analysis of the light-responsive gripper reveals fast actuation to low-intensity light and the opportunity to program deformation states which are stable for minutes without constant illumination. Additionally, through fluid–structure interaction (FSI) simulations, we shed light on the fluid flow induced by the polyp and analyze how design adjustments can improve target attraction through flow control.

Results and Discussion

Design Concept. The artificial polyp integrates two stimuli-responsive materials that are orthogonally addressed to trigger separate actions, allowing for two different modes of motion: rotation of the stem and bending/unbending of the light-responsive arms. The flexible magnetic stem is fabricated following a previously described procedure (32), having a diameter of 1 mm and a length of 6 mm. For stability, the stem is attached to a static transparent PDMS base that is 2 mm thick. Stirring through movement of the magnetic stem (Fig. 1 *C*, *i*) is controlled with a rotating magnet underneath the structure (33). The grasping arms of the artificial polyp are composed of two orthogonally placed strips of LCN films doped with a diacrylate azobenzene chromophore (A1 in Fig. 1*B*) which are attached to each other and to the stem with a drop of ultraviolet (UV)-curable glue. The LCN strips are 1.2 cm long and 0.2 cm wide; the fabrication of the films is described in *Materials and Methods*. Light-responsive contraction originates from the azobenzene molecules isomerizing from stable *trans* to the bent *cis* state upon UV light irradiation. The reverse *cis–trans* isomerization is triggered by irradiation with blue light (see *SI Appendix*, Fig. S1 for the absorbance profile of the azobenzene). Upon UV irradiation from the top of the polyp, the LCN segments bend toward the light source and can capture a passing target, whereas reverse opening actuation and subsequent release of the target is triggered by exposure to blue light (Fig. 1 *C*, *ii*). The LCNs have a planar alignment so as to obtain a rest /no illumination state in which the gripper is in its open configuration (Fig. 1*B*).

Light-Driven Actuation Performance in Water. Planar alignment of the LCNs composing the polyp's gripper results in an open rest state and closure upon illumination with 365-nm light. To characterize the bending actuation of the LCNs and find the optimum concentration for fast and controlled bending, we performed a systematic study of films (2 cm long, 0.5 cm wide, and 20 μm thick) containing 2, 5, and 10 mol % of the diacrylate chromophore for absorbance spectra (see *SI Appendix* for methodology and *SI Appendix*, Fig. S2). First we demonstrate that at a low azo content (2 mol %) negligible actuation is observed, independent of the UV light intensity (Fig. 2*A*). We explain the absence of actuation by the lack of a light absorption gradient through the thickness of the network. With a low content of azobenzene molecules absorbing light on the irradiated side of the film, light penetrates to the back of the film and *trans*-to-*cis* isomerization happens throughout the whole film. Higher concentrations (5 and 10 mol %) show high amplitudes of maximum deformation, with maximum amplitudes in less than 3 s of illumination and nearly independent of the UV light intensity (see also Fig. 2 *B* and *C*). With a high content of azobenzene in the network, nearly all light is absorbed in the first few microns of the film and this "shades" the back side of the strip, leaving the irradiated side of the strip *cis* state-rich and the back *trans* state-rich (34). The different concentrations of the azobenzene isomers on either side of the bilayer create a strain gradient through the thickness which results in the bending of a rectangular film toward the light source, with the *cis*-rich surface on the inside of the bend.

Even though the maximum tip displacements obtained with 5 or 10 mol % azobenzene are similar, the actuation time profile of the films is significantly different (Fig. 2 *B* and *C*). The overall

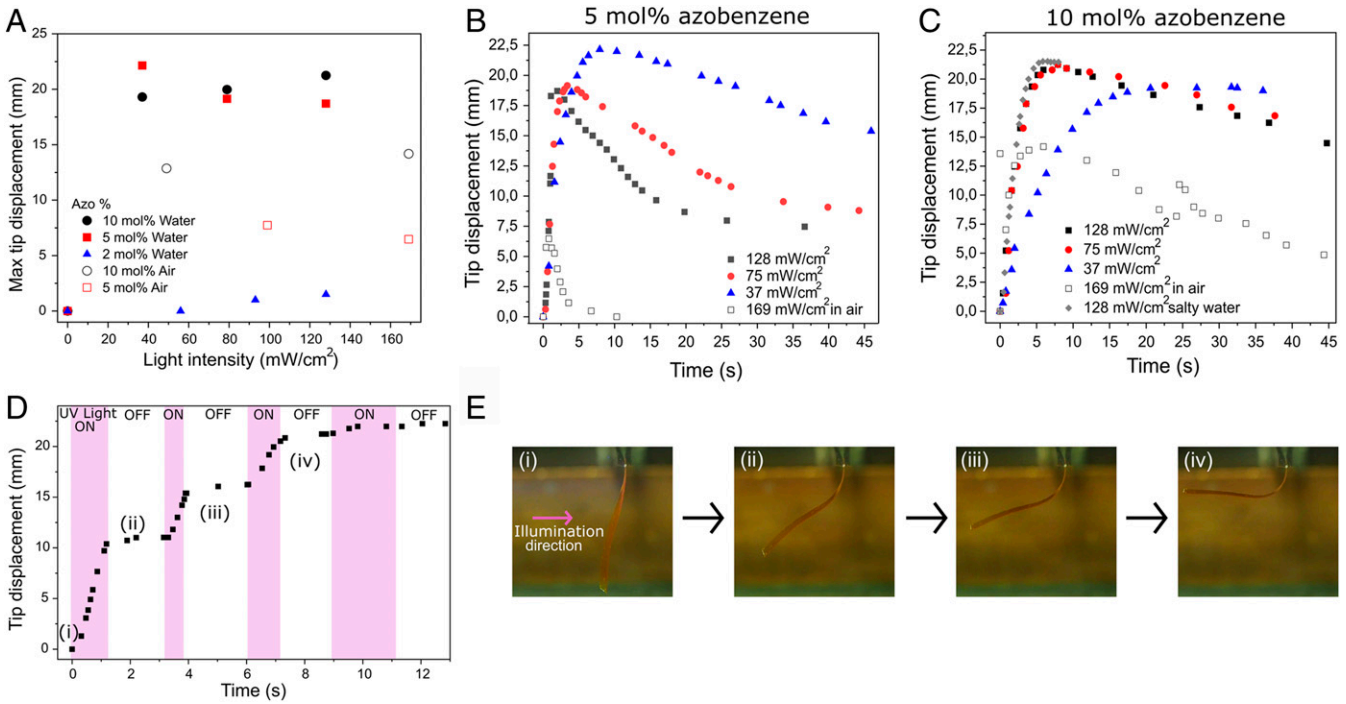

Fig. 2. Characterization of light-driven deformation of planar LCNs in water. (*A*) Maximum tip displacement of planar aligned LCNs with different azobenzene concentrations (2, 5, and 10 mol %) in either water or air. (*B* and *C*) Displacement profile of 5 mol % (*B*) and 10 mol % (*C*) films over time upon irradiation with UV light. (*D*) Light-driven deformation of an azo-containing (10 mol %) planar LCN upon exposure to UV light underwater. Upon ceasing UV light irradiation, the actuator retains its deformed state. (*E*) Photograph snapshots of the LCN strip (2 cm long) at different moments in the actuation; the photographs correspond to the plot in Fig. 1*D*.

actuation trend is a fast displacement during the first seconds of irradiation followed by a decay in the displacement (return to a flatter geometry) under prolonged exposure; see Movie S1 for the underwater actuation of a 10 mol % film upon UV light irradiation (128 mW/cm^2). The decay in the displacement is more distinct for 5 mol % azobenzene films, with higher light intensities leading to faster reverse bending. The reverse bending can be explained referring to the *cis–trans* gradient within the film. Upon prolonged exposure, the gradient advances through the network until light penetrates through the entire thickness and the strain gradient between the active "pulling" *cis* states and the *trans* states is no longer active (34–36). Higher light intensities lead to faster propagation of the *cis–trans* gradient. Higher azobenzene concentration (10 mol %) significantly slows down the propagation of the *trans–cis* boundary (37) so that only prolonged illumination times (>20 s) will lead to considerable decreases in the tip displacement (Fig. 2*C*). Additionally, we demonstrate that unlike hydrogel actuators the LCN film is not sensitive to salt contaminants in the water and can be actuated in the presence of sodium chloride (3.5 weight % in aqueous volume) without any limitations (Fig. 2*C*).

Ceasing UV light exposure results in a temporarily stable deformation. We demonstrate the possibility to accurately control the degree of deformation for temporarily stable bent geometries (time [*t*] >1 h), in which the light exposure time determines the degree of bending (Fig. 2 *D* and *E*). The stable geometry is due to the long *cis* lifetime (*t* >10 h) (22) of the azobenzene which maintains the *cis–trans* gradient, and hence also the macroscopic deformation. Near-complete restoration of the *trans* population is triggered by blue light irradiation, which returns the film to a near-flat geometry. After blue light exposure, the LCN film is not completely flat due to the isomer content at the photostationary state, containing a higher *cis* isomer population than in the non-illuminated/rest state, as blue light is absorbed by both *trans* and *cis* isomers. A completely flat state is only observed after extended times without illumination (22). The opportunity to control a temporary stable deformed state allows for tuning of the geometry of an underwater actuator, with no stimulus required to maintain it. This behavior also differs from previously reported in-water light-responsive hydrogels which require continuously pulsed light to preserve a deformation (18). It should be noted that the ability to control a single stable geometry has been shown for LCNs functioning in dry environments, in which fluorinated azobenzenes with long *cis* lifetimes were used (38, 39). To obtain shape stability in liquid crystalline actuators in air, hydrazone photoswitches have also been utilized (40).

Light-Driven Actuation Comparison in Dry and Aqueous Environments. To further characterize and understand the aqueous actuation of the LCNs, the photo-driven actuation in both aqueous and dry environments is compared (see *Materials and Methods* for methodology). Unlike most hydrogel actuators, the liquid crystalline films utilized in the artificial polyp also function in a dry environment. Previous studies have shown that the in-water actuation of splay aligned films, containing the same diacrylate chromophore A1 as used in this work, are highly diminished when compared to actuation in air (22). However, for planar aligned films, we find the opposite: In aqueous environments actuation is higher (Fig. 2 *A–C* and *SI Appendix*, Fig. S3). Azobenzene-containing LCNs such as splay also actuate as a response to the heat released upon light irradiation of the azobenzene dyes (22). For actuation in water, light-induced heating of the LCNs can be neglected due to heat loss to the surrounding water. We observe that the rate of actuation, which is controlled by the *trans–cis* isomerization kinetics, remains largely unchanged whether actuation is performed in water or in air, even though the fluid medium offers a higher resistance to motion. The greatest difference in the actuation is the higher amplitude

reached when films are irradiated underwater. We attribute it to the lack of heat-promoted back-relaxation of azobenzene moieties, due to absence of film heating underwater. This allows for a higher content of *cis* isomers in the photostationary state and hence for a steeper strain gradient to develop through the film, leading to stronger actuation. The phenomenon of photobleaching, which causes reverse actuation upon prolonged illumination, is present in both wet and dry media; however, in water it is slightly delayed (*SI Appendix*, Fig. S3).

Aquatic Gripper. The four-armed gripper of the artificial polyp is created by combining two rectangular LCN films containing 10 mol % azobenzene. Activation by UV light directed from the top closes the LCN gripper and blue light reopens it (Fig. 3*A*). The diameter of the closed gripper can be programmed by the duration of UV light exposure. As elucidated previously, photoactuation is highly dependent on the illumination time (Fig. 2*D*), so that the degree of bending of the LCN film can be easily controlled with knowledge of the actuation kinetics. Upon removal of UV light the gripper remains in its temporary state and can be further closed by UV light or reopened with blue light (Fig. 3*B*).

Artificial Polyp Wireless Target Attraction, Capture, and Release. We demonstrate how the artificial polyp can be employed as an underwater gripper to grasp or release an object present in the fluid (Movies S2 and S3). The fluid and object used in the demonstration are a water/isopropanol solution and droplets of olive oil (visible in the transparent solution as yellow droplets and neutrally buoyant). The height of the droplets was regulated by altering the ratio between water and isopropanol (~1:1). The artificial polyp is placed on the bottom of a glass container (diameter 2.5 cm), positioned off-center at 0.8 cm from the container wall. The container is filled with the solution up to a height of 2 cm, and stirring is initiated through motion of the magnetic-responsive flexible stem by rotation of a magnet underneath the structure (23). For object capture we demonstrate that the device does not need to be externally guided to a target; instead, it can attract them toward itself through self-induced flow in the liquid (Fig. 4 *A*, *I* and *B*, *i*). Subsequent UV light irradiation triggers the gripper to close, capturing the object (Fig. 4 *B*, *ii*). Once the UV light is switched off the gripper remains in its closed state, enclosing the target (Fig. 4 *B*, *iii*). Furthermore, the reverse demonstration of target release and magnetic-induce fluid flow is also achievable by exposure to blue light (Fig. 4 *A*, *ii* and *B*, *iv*). We envision that such systems can be expanded to realize selected target capture in fluids without the requirements of direct manipulation or intervention in the environment. We note that after blue light exposure the polyp's LCN gripper does not return to a fully flat geometry but retains some degree of bending, with an angle of around 50°.

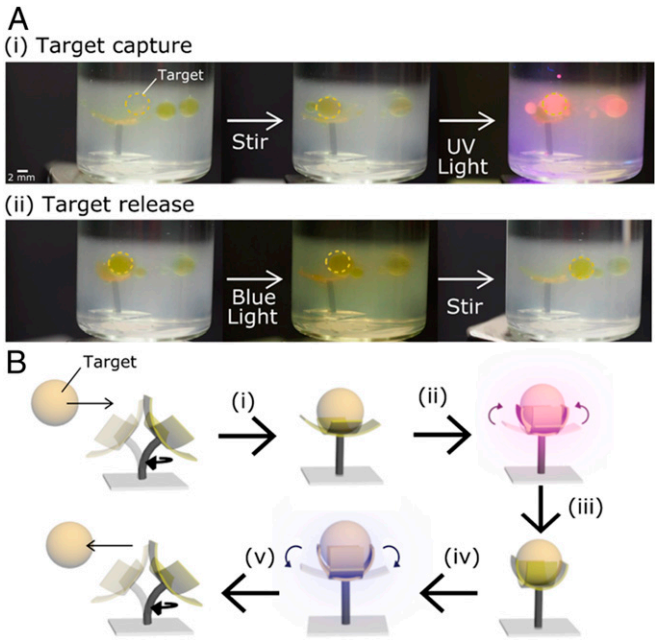

Fig. 4. Artificial polyp in action. (*A*) Photographs showing the magnetic-driven attraction of suspended oil droplets toward the artificial polyp. Motion of the flexible stem is triggered by a magnet rotating underneath the structure at 300 rpm. Target capture is performed through UV light irradiation (*i*) and target release is triggered by blue light (*ii*). (*B*) Schematic depiction of the actuation steps for attraction, capture, and release of a target underwater.

Magnetic-Driven Fluid Flow. To understand the flow-induced attraction of suspended objects toward the artificial polyp, FSI simulations were carried out using a computer design representing the experimental setup (Fig. 5*A*). The suspended oil droplets are not included in the simulations to avoid extensive simulation times. The design consists of a finite container measuring 2.5 cm in diameter filled with fluid up to a height of 2 cm, in which the artificial polyp is positioned off-center, 3 mm from the center of the container. For further details see *SI Appendix, Simulation Methodology*. The velocity field in a horizontal plane 3 mm above the end of the polyp's stem, obtained from the FSI simulations, shows that the moving polyp creates a general spiraling fluid flow directed toward itself (Fig. 5*B*), confirming experimental observations (Movie S4). The polyp-generated flow is not homogeneous but has local velocity maxima near the LCN gripper, located above the four ends of the gripper arms. The

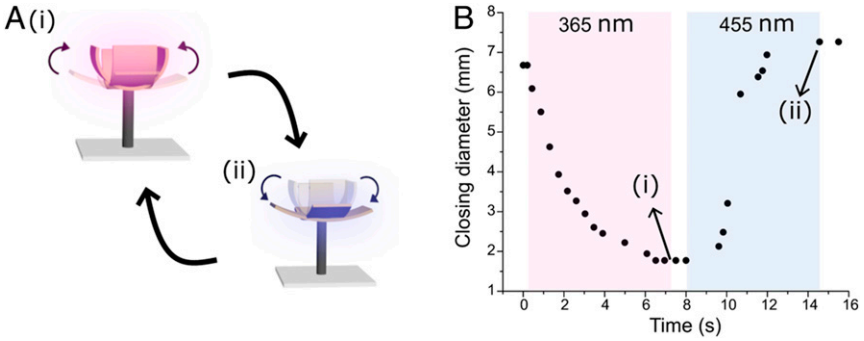

Fig. 3. Light-driven artificial polyp. (*A*) Light-driven reversible deformation of polyp-like design with the gripper composed of two orthogonally placed LCNs (10 mol % azobenzene) upon exposure to (*i*) UV and (*ii*) blue light. (*B*) Analysis of the closing diameter of the gripper upon exposure to UV light (75 mW/cm^2). Ceasing UV light exposure results in a stable closed state. Reopening is triggered by blue light.

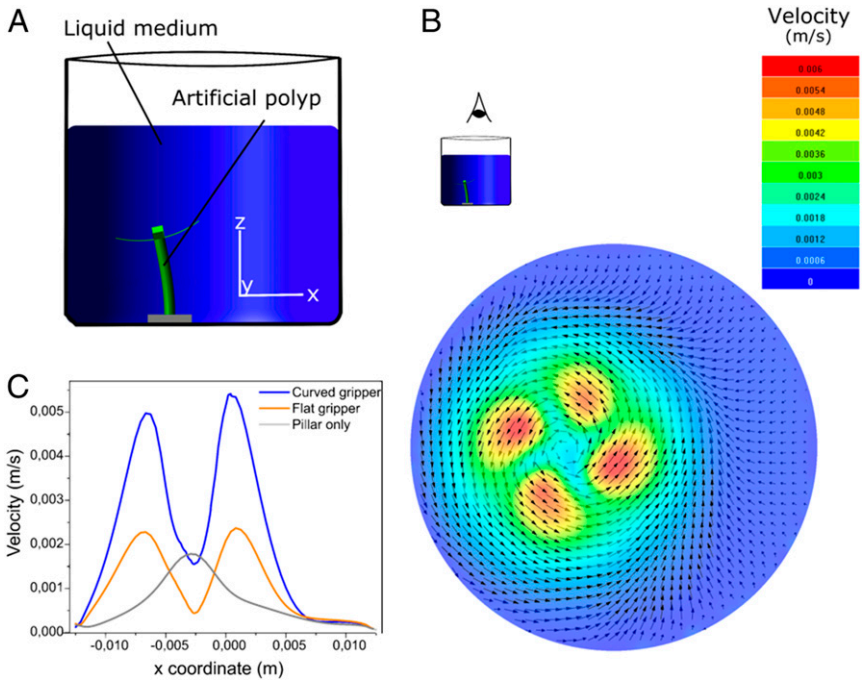

Fig. 5. Simulations of the flow induced by the artificial polyp. (*A*) Computer design used for the simulations. (*B*) Simulated velocity field of the fluid flow induced by the artificial polyp at 3 mm above the end of the magnetic stem in an instantaneous snapshot after 20 rotations of the polyp. The colors indicate the magnitude of the velocity, and the arrows represent the velocity vectors projected on the *x-y* plane. The velocity field moves with the polyp movement, so that the maximum velocity areas are always located above the gripper's end. (*C*) Fluid velocity profile 3 mm above the stirring element (either polyp or sole pillar) along the *x* coordinate (as depicted in *A*).

fluid flow will affect the position of suspended objects; objects further away from the polyp experience lower flow velocities, causing them to circle around the polyp, moving slowly toward it due to the inward spiraling flow. When the magnet rotation rate is increased from 300 rpm to 400 or 600 rpm, the flow fields are identical but the magnitude of the fluid velocities increases respectively (*SI Appendix*, Figs. S4 and S5). After the object has arrived near the gripper it can be captured by light actuation. However, if the gripper is not activated, the flow pattern right above the gripper may temporarily repel the object—depending on the exact location of the object within the velocity field—after which it is attracted again due to the general inward spiraling flow. This behavior can be seen in Movie S4. The simulation movie, Movie S5, shows that as the polyp continuously moves the flow pattern moves with the polyp but does not greatly change, and the attractive flow toward the polyp remains the predominant flow.

Additionally, we explore the effect on the fluid flow dynamics of the gripper's degree of bending, which can be set due to the multistability of the LCN, by comparing a flat gripper, in which the bending angle of the LCN films is 0°, to a slightly bent (50°) gripper (*SI Appendix*, Fig. S6). Additionally, the flow generated by these polyps is compared to that of a simple pillar shape. The velocity profiles corresponding to these three scenarios are shown in Fig. 5*C*. The plot demonstrates that while a simple stirring pillar shows a single maximum in its velocity plot (directly above the pillar; *SI Appendix*, Fig. S7), both polyp designs show maxima above the LCN ends; see *SI Appendix*, Fig. S8 for the simulated velocity field for the flat gripper geometry. The bent gripper induces higher local fluid velocities, 0.0055 m/s compared to 0.002 m/s for a flat gripper, while being sufficiently open to allow a target to enter its grip. The general inward spiraling flow is induced for all three geometries, as seen in Fig. 5*B* and *SI Appendix*, Figs. S7 and S8. These simulation results not only show that the flow patterns are very dependent on the geometry of the mixing element (polyp vs. pillar) but also that the flow velocity can be directly controlled by light, not only by changing the magnet rotation speed.

Conclusions

Inspired by autonomous marine organisms that attract and capture suspended targets, we have presented an artificial polyp that can be remotely controlled to generate fluid flow and capture or release targets. The design integrates two different stimuli-responsive materials, a flexible magnetic PDMS pillar and light-responsive LCPs. The independent device segments can be orthogonally controlled to realize different functions including magnetic-driven stirring and light-triggered gripping within the same device. Eliminating the need of guiding the gripper to a target with an external tether realizes a fully wirelessly driven device. Additionally, the amphibious actuation of the light-responsive polyp's gripper allows for operation in diverse environments including dry and aqueous, making it unique in the field of light-responsive soft grippers. The light-responsive polymer films show rapid actuation underwater (t <3 s) even to low-intensity light (<40 mW/cm^2), insensitivity to salt contaminants in the water, and multistable deformation geometries. These qualities make azobenzene-doped LCNs a promising alternative to conventionally used hydrogel materials for in-water applications. The LCN and the azobenzene derivative utilized have been commonly used for soft robotics operating in a dry environment, and we hereby demonstrate the potential of already existing materials in novel applications. Simulations of the fluid flow generated by the artificial polyp enables visualization and quantification of the flow fields developed and shed light on how the polyp's design affects the stirring pattern. The simulations particularly provide guidelines to how the multishape stability of the LCN grippers can be utilized to tune the gripper's shape to enhance the polyp's flow induced attraction of targets. Overall, by combining two different stimuli-responsive materials in a single soft robotic device, we demonstrate how assemblies of

soft materials can expand device functionality and allow for completion of tasks that would not be possible utilizing single-component devices.

Materials and Methods

Fabrication of LCN Films. The LCP networks utilized in this study are fabricated through the photopolymerization of liquid crystalline monomers, a diacrylate, (LC mesogen, RM82; Merck) and an azobenzene chromophore, (A1, A6A; SYNTHON Chemicals GmbH), initiated by a photoinitiator (Irgacure 819, 1 mol %: Ciba). Prior to polymerization, the monomers are dissolved in dichloromethane to obtain a homogeneous mixture, and subsequently the solvent is evaporated. Polymerization is done in a glass cell, made by gluing two glass slides coated with a polyimide alignment layer (Optimer AL1051; JSR Mircro) using UV-curable glue containing 20-μm glass bead spacers. Cell filling is done at 110 °C; at this temperature the LC mixture is isotropic. The filled cell is then cooled to 95 °C, at which temperature the LC mixture is nematic. Photopolymerization is done for 15 min, using an Exfo Omnicure S2000 lamp. A cutoff filter ($\lambda \geq 400$ nm, FGL400S; Thorlabs is used during polymerization. A thermal treatment at 120 °C for 10 min releases thermal stresses that arise from polymer shrinkage during polymerization. After polymerization, the cell is opened, and the films are peeled from the glass with razor blades and cut into strips, in which the alignment direction of the planar side is parallel to the long side of the film. The cut strips are 2 cm long and 0.5 cm wide.

Actuation Analysis of Light-Responsive LCN Films. Actuation analysis is carried out using two light-emitting diodes (LEDs), 365 nm (M365L2; Thorlabs) and 455 nm (M455L3) equipped with a collimator to focus the light (SM2F32-A). The LEDs are controlled using a current-driven DC4104 from Thorlabs. The lights are positioned around 10 cm away from the films. Tap water (18 °C) is used for the in-water actuation. We assume an isothermal environment, as any temperature increase of the film during illumination would immediately be lost to the aqueous surrounding. We have used a thermometer to track the water temperature in the vicinity of the film during illumination and observed a maximum 1 to 2 °C increase. For in-water actuation analysis we correct for any light absorbed by the water before reaching the sample. We measured that for blue light 14% of the light is absorbed before reaching the sample and for UV light this is 24% (22).

Simulation Methodology. Three-dimensional models of the experimental setup were constructed using SolidWorks (Dassault Systèmes) and the FSI simulations were performed using Abaqus/Explicit (Dassault Systèmes) and FlowVision (Capvidia). To represent the structural aspects of the FSI simulations, the pillar was meshed using 22,500 high-quality C3D8R elements while the LCN gripper, which was assumed to be rigid, was meshed with 1,678 R3D4 elements using Abaqus CAE (Dassault Systèmes). The pillar was assumed to be an isotropic linear elastic material with Young's modulus of 3 MPa and a Poisson ratio of 0.45. The rigid gripper and the deformable pillar were tied to one another using Abaqus' inbuilt tie constraint. The experimentally observed "swinging" motion of the pillar was simulated realistically using appropriate displacement boundary conditions. The bottom of the pillar was constrained so that it had zero degrees of freedom. A node lying at the center of the top face of the pillar was selected and circular boundary conditions were prescribed for this node with time-dependent x and y amplitude of $1 \times \cos(2\pi t/T)$ and $1 \times \sin(2\pi t/T)$, respectively, which means that the radius of the circular motion was set to 1 mm, consistent with the experiments, and T is the time period the pillar takes to complete one complete revolution. In this investigation, T was taken to be 0.2 s, which corresponds to rpm of 300 (as in the experiments). Finally, a user-defined surface was created within Abaqus/Explicit on the pillar and the gripper which acts as a fluid–structure interface facilitating the exchange of information between the structural and the flow solver. Fluid flow due to the FSI was simulated by solving the incompressible Navier–Stokes equations coupled with the volume-of-fluid approach to account for the free surface phenomena. Water was selected as the working fluid with a dynamic viscosity of 0.00182 Pa·s and a density of 999.84 kg/m^3. The fluid domain was discretized into 251,000 high-quality Cartesian and polyhedral cells with adaptive refinement on the moving structures, that is, pillar and gripper. No-slip boundary conditions were prescribed throughout the domain and the fluid motion was induced due to the swinging motion of the pillar and the gripper. Abaqus/Explicit and FlowVision were coupled explicitly and both solvers exchanged displacement and force data at a user-defined time interval of 1×10^{-4} s. Simulations were performed for a total time span of 4.05 s with a time step of 1×10^{-7} s and 1×10^{-4} s in Abaqus/Explicit and FlowVision, respectively. The extremely fine time step for Abaqus/Explicit was chosen to ensure quasi-static behavior of the pillar.

Data Availability. All data, materials, and associated protocols that support the findings of this study are shown in *Materials and Methods* and *SI Appendix*.

ACKNOWLEDGMENTS. We thank Shuaizhong Zhang for the fabrication of the magnetic-responsive pillars and acknowledge financial support from the Impuls II grant from the Eindhoven University of Technology.

1. S. I. Rich, R. J. Wood, C. Majidi, Untethered soft robotics. *Nat. Electron.* **1**, 102–112 (2018).
2. D. Rus, M. T. Tolley, Design, fabrication and control of soft robots. *Nature* **521**, 467–475 (2015).
3. M. Pilz da Cunha *et al*., A soft transporter robot fueled by light. *Adv. Sci. (Weinh.)* **7**, 1902842 (2020).
4. C. Huang *et al*., Miniaturized swimming soft robot with complex movement actuated and controlled by remote light signals. *Sci. Rep.* **5**, 17414 (2015).
5. W. Hu, G. Z. Lum, M. Mastrangeli, M. Sitti, Small-scale soft-bodied robot with multimodal locomotion. *Nature* **554**, 81–85 (2018).
6. Y. Zhao *et al*., Soft phototactic swimmer based on self-sustained hydrogel oscillator. *Sci. Robot.* **4**, 1–11 (2019).
7. M. Sitti, Miniature soft robots–Road to the clinic. *Nat. Rev. Mater.* **3**, 74–75 (2018).
8. C. Yao *et al*., Poly(N-isopropylacrylamide)-clay nanocomposite hydrogels with responsive bending property as temperature-controlled manipulators. *Adv. Funct. Mater.* **25**, 2980–2991 (2015).
9. E. Palleau, D. Morales, M. D. Dickey, O. D. Velev, Reversible patterning and actuation of hydrogels by electrically assisted ionoprinting. *Nat. Commun.* **4**, 2257 (2013).
10. J. Zheng *et al*., Mimosa inspired bilayer hydrogel actuator functioning in multi-environments. *J. Mater. Chem. C* **6**, 1320–1327 (2018).
11. C. Ma *et al*., A multiresponsive anisotropic hydrogel with macroscopic 3D complex deformations. *Adv. Funct. Mater.* **26**, 8670–8676 (2016).
12. M. Wei, Y. Gao, X. Li, M. J. Serpe, Stimuli-responsive polymers and their applications. *Polym. Chem.* **8**, 127–143 (2017).
13. H. Zeng, P. Wasylczyk, D. S. Wiersma, A. Priimagi, Light robots: Bridging the gap between microrobotics and photomechanics in soft materials. *Adv. Mater.* **30**, e1703554 (2017).
14. C. Yoon, Advances in biomimetic stimuli responsive soft grippers. *Nano Converg.* **6**, 20 (2019).
15. L. Ionov, Hydrogel-based actuators: Possibilities and limitations. *Mater. Today* **17**, 494–503 (2014).
16. J. Shang, X. Le, J. Zhang, T. Chen, P. Theato, Trends in polymeric shape memory hydrogels and hydrogel actuators. *Polym. Chem.* **10**, 1036–1055 (2019).
17. J. Chen *et al*., Artificial muscle-like function from hierarchical supramolecular assembly of photoresponsive molecular motors. *Nat. Chem.* **10**, 132–138 (2018).
18. S. Coleman *et al*., Tuning microfluidic flow by pulsed light oscillating spiropyran-based polymer hydrogel valves. *Sens. Actuators B Chem.* **245**, 81–86 (2017).
19. Z. C. Jiang, Y. Y. Xiao, Y. Zhao, Shining light on liquid crystal polymer networks: Preparing, reconfiguring, and driving soft actuators. *Adv. Opt. Mater.* **7**, 1900262 (2019).
20. X. Pang, J. Lv, C. Zhu, L. Qin, Y. Yu, Photodeformable azobenzene-containing liquid crystal polymers and soft actuators. *Adv. Mater.* **31**, 1904224 (2019).
21. C. L. van Oosten, C. W. M. Bastiaansen, D. J. Broer, Printed artificial cilia from liquid-crystal network actuators modularly driven by light. *Nat. Mater.* **8**, 677–682 (2009).
22. M. Pilz da Cunha, E. A. J. van Thoor, M. G. Debije, D. J. Broer, A. P. H. J. Schenning, Unravelling the photothermal and photomechanical contributions to actuation of azobenzene-doped liquid crystal polymers in air and water. *J. Mater. Chem. C* **7**, 13502 (2019).
23. O. M. Wani, H. Zeng, A. Priimagi, A light-driven artificial flytrap. *Nat. Commun.* **8**, 15546 (2017).
24. H. Shahsavan *et al*., Bioinspired underwater locomotion of light-driven liquid crystal gels. *Proc. Natl. Acad. Sci. U.S.A.* **117**, 5125–5133 (2020).
25. M. Kremien, U. Shavit, T. Mass, A. Genin, Benefit of pulsation in soft corals. *Proc. Natl. Acad. Sci. U.S.A.* **110**, 8978–8983 (2013).
26. O. H. Shapiro *et al*., Vortical ciliary flows actively enhance mass transport in reef corals. *Proc. Natl. Acad. Sci. U.S.A.* **111**, 13391–13396 (2014).
27. J. E. Samson, N. A. Battista, S. Khatri, L. A. Miller, Pulsing corals: A story of scale and mixing. *Biomath (Sofia)* **6**, 1712169 (2017).
28. T. G. Leong *et al*., Tetherless thermobiochemically actuated microgrippers. *Proc. Natl. Acad. Sci. U.S.A.* **106**, 703–708 (2009).
29. K. Kobayashi, C. Yoon, S. H. Oh, J. V. Pagaduan, D. H. Gracias, Biodegradable thermomagnetically responsive soft untethered grippers. *ACS Appl. Mater. Interfaces* **11**, 151–159 (2019).
30. S. Won, S. Kim, J. E. Park, J. Jeon, J. J. Wie, On-demand orbital maneuver of multiple soft robots via hierarchical magnetomotility. *Nat. Commun.* **10**, 4751 (2019).

31. F. Ongaro *et al*., Autonomous planning and control of soft untethered grippers in unstructured environments. *J. Microbio Robot.* **12**, 45–52 (2017).
32. S. Zhang, Y. Wang, P. R. Onck, J. M. J. den Toonder, Removal of microparticles by ciliated surfaces—An experimental study. *Adv. Funct. Mater.* **29**, 1–11 (2019).
33. A. Saberi *et al*., A stirring system using suspended magnetically-actuated pillars for controlled cell clustering. *Soft Matter* **15**, 1435–1443 (2019).
34. C. L. Van Oosten *et al*., Bending dynamics and directionality reversal in liquid crystal network photoactuators. *Macromolecules* **41**, 8592–8596 (2008).
35. M. Kondo *et al*., Effect of concentration of photoactive chromophores on photomechanical properties of crosslinked azobenzene liquid-crystalline polymers. *J. Mater. Chem.* **20**, 117–122 (2010).
36. A. Shimamura *et al*., Simultaneous analysis of optical and mechanical properties of cross-linked azobenzene-containing liquid-crystalline polymer films. *ACS Appl. Mater. Interfaces* **3**, 4190–4196 (2011).
37. C. Li, J. H. Yun, H. Kim, M. Cho, Light propagation and photoactuation in densely cross-linked azobenzene-functionalized liquid-crystalline polymers: Contribution of host and concerted isomerism. *Macromolecules* **49**, 6012–6020 (2016).
38. S. Iamsaard *et al*., Fluorinated azobenzenes for shape-persistent liquid crystal polymer networks. *Angew. Chem. Int. Ed. Engl.* **55**, 9908–9912 (2016).
39. M. Hendrikx *et al*., Re- and preconfigurable multistable visible light responsive surface topographies. *Small* **14**, e1803274 (2018).
40. A. Ryabchun, Q. Li, F. Lancia, I. Aprahamian, N. Katsonis, Shape-persistent actuators from hydrazone photoswitches. *J. Am. Chem. Soc.* **141**, 1196–1200 (2019).